

Absorbing Boundaries for the Nonlinear Schrödinger Equation

A. Soffer and C. Stucchio

May 25, 2019

Abstract

We present a new algorithm, the Time Dependent Phase Space Filter (TDPSF) which is used to solve time dependent Nonlinear Schrödinger Equations (NLS). The algorithm consists of solving the NLS on a box with periodic boundary conditions (by any algorithm). Periodically in time, we decompose the solution into a family of coherent states. Those coherent states which are outgoing are deleted, while those which are not are kept, thus minimizing the problem of reflected (wrapped) waves. Numerical results are given, and rigorous error estimates are described.

1 Introduction and Definitions

Consider a semilinear Schrödinger equation on \mathbb{R}^{N+1}

$$i\partial_t\psi(x,t) = -(1/2)\Delta\psi(x,t) + g(t,\vec{x},\psi(\vec{x},t))\psi(\vec{x},t) \quad (1.1)$$

where $g(t,\vec{x},\cdot)$ is some semilinear perturbation. For instance, $g(t,\vec{x},\cdot)$ could be $V(\vec{x},t) + f(|\psi(\vec{x},t)|^2)$ for some smooth function f and (spatially) localized potential $V(\vec{x},t)$. Abusing terminology, we refer to $g(t,\vec{x},\cdot)$ as the nonlinearity even when it is linear.

We assume the initial condition and nonlinearity are such that the nonlinearity remains localized inside some box $[-L_{\text{NL}}, L_{\text{NL}}]^N$. Outside this region the solution is assumed to behave like a free wave.

One very common method of solving such a problem is domain truncation. That is, one solves the PDE (1.1) numerically on a region $[-L, L]^N$. On the finite domain, boundary conditions must be specified. Dirichlet or Neumann boundaries introduce spurious reflections, while periodic boundaries allow outgoing waves to wrap around the computational domain. This causes the numerical solution to become incorrect after a time $T \approx L/k_{\text{max}}$, where k_{max} is the “maximal velocity” (the highest relevant spatial frequency) of the solution.

There are two main approaches to dealing with this problem. One approach, the Dirichlet-to-Neumann method, consists of attempting to use the exact solution as a boundary condition. Although this works rather well for the wave

equation [1, 2, 11, 13, 15], it is fraught with problems for dispersive waves and only limited progress has been made [18, 21, 22, 28]. Dirichlet-to-Neumann methods also prevent the use of fast spectral methods for solving the interior problem because spectral methods based on the FFT naturally impose periodic boundary conditions.

A simpler idea is to add a dissipative term which is localized near the boundary, on a region $[-(L_{\text{int}} + w), (L_{\text{int}} + w)]^N \setminus [-L_{\text{int}}, L_{\text{int}}]^N$. The dissipative term can be an absorbing potential [19] or the more sophisticated PML [3]. Either way, the part of the solution on the boundary region is dissipated. This dissipates outgoing waves, but it also dissipates incoming waves located near the boundary. This can introduce spurious dissipation (see Section 3.2), which the TDPSF does not have.

1.1 Our Approach

We propose an alternative approach to absorbing boundaries. Suppose we want to approximate the solution in the space H^s (with s large enough to make (1.1) is well posed). We make the assumption that near the boundary of the box, the solution behaves like a free wave. That is, outside some region $[-L_F, L_F]^N$, $\psi(x, t)$ behaves like a free wave, i.e. $\psi(x, t) \approx e^{i(1/2)\Delta t}\psi_+(x)$. The number L_F is chosen to be a large enough number so that this holds.

We assume the nonlinearity is nearly localized both in position and momentum. That is, we assume the existence of $L_{\text{NL}}, k_{\text{max,NL}}$ so that:

$$\left\| [1 - \chi_{[-L_{\text{NL}}, L_{\text{NL}}]^N}(\vec{x})]g(t, \vec{x}, \psi(x, t))\psi(x, t) \right\|_{H^s} \approx 0 \quad (1.2a)$$

$$\left\| [1 - \chi_{[-k_{\text{max,NL}}, k_{\text{max,NL}}]^N}(\vec{k})]g(t, \vec{x}, \psi(x, t))\psi(x, t) \right\|_{H^s} \approx 0 \quad (1.2b)$$

For technical reasons, we assume that the nonlinearity is Lipschitz in H^s , although we believe this can be relaxed. In particular, the nonlinearity could take the form of a time dependent short range potential $V(\vec{x}, t)\psi(\vec{x}, t)$ or a local nonlinearity $f(|\psi(\vec{x}, t)|^{2\sigma})\psi(\vec{x}, t)$ with $f(z)$ a bounded function.

We also assume that the solution remains localized in frequency, that is the H^s norm of $\hat{\psi}(\vec{k}, t)$ is small outside $[-k_{\text{max}}, k_{\text{max}}]^N$ for some large number k_{max} (the maximal momentum of the problem, which we assume exists).

Our algorithm is as follows. We assume the initial data is localized on a region $[-L_{\text{int}}, L_{\text{int}}]^N$. We solve (1.1) on the box $[-(L_{\text{int}} + w), L_{\text{int}} + w]^N$ on the time interval $[0, T_{\text{step}}]$. We insist that $L_{\text{int}} > L_F, L_{\text{NL}}$ so that the solution behaves like a free wave on $[-(L_{\text{int}} + w), (L_{\text{int}} + w)]^N \setminus [-L_{\text{int}}, L_{\text{int}}]^N$.

By making T_{step} smaller than $w/3k_{\text{max}}$, we can ensure that $\psi(\vec{x}, T_{\text{step}})$ is mostly localized inside box $[-(L_{\text{int}} + w), (L_{\text{int}} + w)]^N$. Since very little mass has reached the boundary, the error is nearly zero [26, Thm. 4.1].

We then decompose $\psi(\vec{x}, T_{\text{step}})$ into a sum of gaussians (indexed by $\vec{a}, \vec{b} \in \mathbb{Z}^N$, with lattice spacing x_0 in position, k_0 in momentum and standard deviation

σ):

$$\psi(x, T_{\text{step}}) \approx \sum_{\substack{|\vec{a}x_0|_\infty \leq L_{\text{int}} + w \\ |\vec{b}k_0|_\infty \leq k_{\text{max}}}} \psi_{(\vec{a}, \vec{b})} \pi^{-N/4} \sigma^{-N/2} e^{ik_0 \vec{b} \cdot \vec{x}} e^{-|\vec{x} - \vec{a}x_0|_2^2 / 2\sigma^2}$$

We then examine the gaussians near the boundary, $|\vec{a}x_0|_\infty \geq L_{\text{int}}$, and determine whether they are leaving the box or not under the free flow ($|\vec{x}|_p$ denotes the l^p norm on finite vectors). By assumption, $e^{i(1/2)\Delta t}$ is a sufficiently accurate approximation to the true solution for this part of the solution. We apply this approximation to each framelet:

$$\begin{aligned} & e^{i(1/2)\Delta t} \pi^{-N/4} \sigma^{-N/2} e^{ik_0 \vec{b} \cdot \vec{x}} e^{-|\vec{x} - \vec{a}x_0|_2^2 / 2\sigma^2} \\ &= \frac{\exp\left(i\vec{b}k_0 \cdot (\vec{x} - (\vec{b}k_0/2)t - \vec{a}x_0)\right)}{\pi^{N/4} \sigma^{N/2} (1 + it/\sigma^2)^{N/2}} \exp\left(\frac{-|\vec{x} - \vec{b}k_0 t - \vec{a}x_0|_2^2}{2\sigma^2(1 + it/\sigma^2)}\right) \quad (1.3) \end{aligned}$$

Under the free flow, a framelet moves along the trajectory $\vec{a}x_0 + \vec{b}k_0 t$ while spreading about its center. If a given gaussian is leaving the box, we delete it (set $\psi_{(\vec{a}, \vec{b})} = 0$). Some gaussians spread more quickly than their center of mass moves, and we do not present here an algorithm to deal with these gaussians.

After this filtering operation, the only gaussians remaining are either inside the box $[-L_{\text{int}}, L_{\text{int}}]^N$, or inside the box $[-(L_{\text{int}} + w), (L_{\text{int}} + w)]^N$ but moving towards $[-L_{\text{int}}, L_{\text{int}}]^N$. Thus, it is safe to propagate for a time T_{step} , since what remains will not hit the boundaries before this time. We do the same at time $2T_{\text{step}}, 3T_{\text{step}}, \text{etc.}$

The main drawback to this approach is that some gaussians are ambiguous. Consider a gaussian with velocity 0: $\pi^{-N/4} \sigma^{-N/2} e^{-|\vec{x} - \vec{a}x_0|_2^2 / 2\sigma^2}$. Suppose also that $\vec{a}x_0$ is located inside $[-(L_{\text{int}} + w), (L_{\text{int}} + w)]^N \setminus [-L_{\text{int}}, L_{\text{int}}]^N$. By examining (1.3), we observe that this framelet is spreading out laterally both into the box and outward. If we delete it, we have removed waves which should have returned. If we fail to delete it, then that part of the framelet which is spreading outwards will wrap around and cause an error.

This happens only for gaussians which are moving slowly relative to the box. Thus, we impose one additional assumption – we assume that gaussians moving so slowly that they move both ways do not occur in the solution.

1.2 Error Bounds

We prove rigorous error bounds for the TDPSF algorithm in [26], as well as stating explicitly the assumptions and defining what we mean by “ \approx ”. Although the error bound is too long to state explicitly here, we describe briefly the form it takes.

For a general time-stepping algorithm (with periodic boundaries and no

filtering), the error bound would take the following form:

$$\begin{aligned} \sup_{t \in [0, T_{\max}]} \|\mathcal{U}(t)\psi_0(x) - \Psi(x, t)\|_{H_b^s} &\leq \text{BoundaryError}(T_{\max}) \\ &+ \text{HighFrequency}(T_{\max}) + \text{LowFrequency}(T_{\max}) \\ &+ \text{NonlocalNonlinearity}(T_{\max}) + \text{Instability}(T_{\max}) \quad (1.4) \end{aligned}$$

The term $\text{BoundaryError}(T_{\max})$ encompasses errors due to waves wrapping/reflecting from the boundaries of the box. For many problems, this is the dominant error term. It is directly proportional to the mass which would have (if we were solving the problem on \mathbb{R}^N) radiated outside the box $[-L_{\text{int}}, L_{\text{int}}]^N$.

The $\text{HighFrequency}(T_{\max})$ part stems from waves with momenta too high to be resolved by the discretization. The term $\text{LowFrequency}(T_{\max})$ encompasses errors due to waves with wavelength that is long in comparison to the box. The term $\text{NonlocalNonlinearity}(T_{\max})$ stems from that fraction of the nonlinearity itself which is located outside the box. The $\text{Instability}(T_{\max})$ stems from the possibility that the dynamics of the solution itself might amplify the other errors dramatically (e.g. in strongly nonlinear problems).

Our algorithm reduces the term $\text{BoundaryError}(T_{\max})$. The other errors are assumed to be small, since we are concerned only with the boundary error at this point.

The method of proof is a direct calculation. We calculate the errors made in the filtering step (decomposition into gaussians), as well as the errors made while propagating in between filtering. We then add up the error over time, taking into account possible instabilities of the system being simulated. The error takes the form described in (1.4). The $\text{BoundaryError}(T_{\max})$ term can be reduced by increasing w , and the error behaves like $\text{BoundaryError}(T_{\max}) = O(e^{-Cw}T_{\max})$. In many cases (problems which are asymptotically complete and have no bound states), we believe that this error can be proved to be time independent.

The main drawback of our algorithm is that it does not provide us the ability to filter waves for which the wavelength is longer than the buffer region. This should not come as a surprise, due to the Heisenberg uncertainty principle. See however Section 5 where we discuss a possible method to deal with this.

2 The Algorithm

2.1 The Windowed Fourier Transform

The discrete windowed Fourier transform frame is a way of localizing a function $f(\vec{x})$ in the phase space. For the big picture, see [8, 10], and also [26, Section 3] and [9] for technical details needed by the TDPSF.

The WFT is an expansion of a function $f(x)$ into the following “basis” (actually a frame) for $L^2(\mathbb{R}^N)$:

$$\phi_{(\vec{a}, \vec{b})}(\vec{x}) = \pi^{-N/4} \sigma^{-N/2} e^{ik_0 \vec{b} \cdot \vec{x}} e^{-|\vec{x} - \vec{a}x_0|_2^2 / 2\sigma^2}, \quad \vec{a}, \vec{b} \in \mathbb{Z}^N \times \mathbb{Z}^N \quad (2.1)$$

The lattice spacing in position and momentum, x_0 , k_0 , and the standard deviation σ must positive real numbers. To be a frame, it must hold that $x_0 k_0 < 2\pi$.

This family of functions is not a basis in the usual sense, but a frame. A family of functions $\{\phi_j(x)\}_{j \in J}$ is a frame in the Hilbert space H if there exists an $0 < A_F \leq B_F < \infty$ so that:

$$A_F \|f(x)\|_H \leq \left(\sum_{j \in J} |\langle f | \phi_j(x) \rangle|^2 \right)^{1/2} \leq B_F \|f(x)\|_H$$

A frame is an overcomplete, non-orthonormal basis with a numerically stable reconstruction procedure. We can then decompose any $f \in L^2(\mathbb{R}^N)$ as:

$$f(\vec{x}) = \sum_{(\vec{a}, \vec{b}) \in \mathbb{Z}^N \times \mathbb{Z}^N} f_{(\vec{a}, \vec{b})} \phi_{(\vec{a}, \vec{b})}(\vec{x}) \quad (2.2)$$

$$f_{(\vec{a}, \vec{b})} = \langle f(\vec{x}) | \tilde{\phi}_{(\vec{a}, \vec{b})}(\vec{x}) \rangle \quad (2.3)$$

The functions $\tilde{\phi}_{(\vec{a}, \vec{b})}(\vec{x})$ are given by $\tilde{\phi}_{(\vec{a}, \vec{b})}(\vec{x}) = e^{ik_0 \vec{b} \cdot \vec{x}} \tilde{g}(\vec{x} - \vec{a}x_0)$ with $\tilde{g}(\vec{x}) \in L^2(\mathbb{R}^N)$ (see [8, 9] for procedures to calculate $\tilde{g}(\vec{x})$).

In [26] we extend the analysis of [9] and show that if $x_0 k_0 = 2\pi/\mathbf{M}$ for $\mathbf{M} \in 2\mathbb{N}$, $g(\vec{x})$ decays exponentially in $|\vec{x}|_1$ and $\hat{g}(\vec{k})$ decays exponentially in $|\vec{k}|_1$:

$$|\partial_x^{\vec{\alpha}} \tilde{g}(\vec{x})| \leq \mathbf{g}(x_0, k_0, N, \vec{\alpha}) e^{-\mathbf{r}(x_0, k_0) |\vec{x}|_1} \quad (2.4)$$

$\mathbf{g}(x_0, k_0, N, \vec{\alpha})$ is a constant (explicitly bounded in [26]) as is $\mathbf{r}(x_0, k_0) = x_0 \mathbf{M}/8\pi\sigma$. (2.4) holds for $\hat{g}(\vec{k})$, but with x_0 and k_0 swapped and σ^{-1} replacing σ .

2.1.1 Phase Space Localization

The WFT allow us to define a concrete realization of phase space. From here onward, we will consider $\mathbb{Z}^N \times \mathbb{Z}^N$ to be a discrete realization of phase space. The vector $(\vec{a}, \vec{b}) \in \mathbb{Z}^N \times \mathbb{Z}^N$ will represent the point at $\vec{a}x_0$ in position, and $\vec{b}k_0$ in momentum.

With this in mind, we can now construct phase space localization operators very simply. For a set $F \in \mathbb{Z}^N \times \mathbb{Z}^N$, we define \mathcal{P}_F by:

$$\mathcal{P}_F \psi(x) = \sum_{(\vec{a}, \vec{b}) \in F} \psi_{(\vec{a}, \vec{b})} \phi_{(\vec{a}, \vec{b})}(\vec{x}) = \sum_{(\vec{a}, \vec{b}) \in F} \phi_{(\vec{a}, \vec{b})}(\vec{x}) \langle \tilde{\phi}_{(\vec{a}, \vec{b})}(\vec{x}) | \psi(x) \rangle \quad (2.5)$$

It can be shown [26, 7, 8] that phase space localization in terms of the WFT corresponds closely (though not exactly) to the usual phase space localization. We state one theorem (proved in [26], based on a result by Daubechies from [7, 8]) as an example of this:

Theorem 2.1 *Let $B_X = [-X, X]^N$, $B_K = [-K, K]^N$ for $X, K < \infty$. Suppose also that $x_0 k_0 = 2\pi/\mathbf{M}$ for $\mathbf{M} \in 2\mathbb{N}$. Then there exists C , \mathbf{X} and \mathbf{K} so that if $X' = X - \mathbf{X}$, $K' = K - \mathbf{K}$, then:*

$$\begin{aligned} & \|f(x) - \mathcal{P}_{B_{X'} \times B_{K'}} f(x)\|_{H^s} \\ & \leq C \left(\|(1 - P_{B_X; x_0}^s(\vec{x}))f(\vec{x})\|_{H^s} + \|(1 - P_{B_K; k_0}^0(\vec{k}))f(\vec{x})\|_{H^s} + \epsilon \|f\|_{H^s} \right) \end{aligned} \quad (2.6)$$

The constant C depends on $\epsilon, s, x_0, k_0, \sigma, X$ and K , as do \mathbf{X} and \mathbf{K} . C is given explicitly in [26].

2.1.2 Computation of the WFT Coefficients and Phase Space Projections: How to do it, and how hard it is

We now present the algorithm for computing the framelet coefficients. The algorithm consists of computing the products $f(\vec{x})\tilde{g}(\vec{x} - \vec{a}x_0)$, followed by Fourier transforming the results. Due to the spatial decay of $\tilde{g}(\vec{x})$, we can truncate the domain to a reasonably small box surrounding $\vec{a}x_0$ with minimal error.

Let `dual_window` be a numerical approximation to $\tilde{g}(\vec{x})$. Let `translate` be the translation operator. Let `kmax` be the maximum resolvable frequency on the given grid (for a uniformly spaced grid, `kmax` = $2\pi/DX$).

Algorithm 2.1 *Calculation of Windowed Fourier Transforms*

```
DualWindow          //A numerical approximation to the Dual Window

def wft_coefficients(grid, arange):
    wft_coefficients = crossProduct(arange, [-kmax, kmax])
    xbuff, kbuff      //xbuff and kbuff are temporary buffers
                      //which are large enough to store DualWindow,
    for a in arange: //but no larger.
        xbuff = multiply(translate(DualWindow, a*x0), grid)
        xbuff = truncate_to_support(xbuff)
        kbuff = FFT(xbuff)
        wft_coefficients[a][:] = kbuff[:]
    return wft_coefficients
```

The function `truncate_to_support(xbuff)` deletes those data points which are outside the support of `DualWindow`. We abuse the term “support”, using it to denote the region where $\tilde{g}(\vec{x})$ is greater than some small tolerance.

We observe that this algorithm is local in space. This means that if `arange` is a finite region, then the computational cost is proportional to:

$$|A| k_{\max}^N |\text{supp } \tilde{g}(\vec{x})|^N \log(k_{\max} |\text{supp } \tilde{g}(\vec{x})|)$$

Here, $A \subset \mathbb{Z}^N$ is the region of space in which we want to compute the WFT coefficients.

The reason for this complexity is as follows. For each $\vec{a} \in A = \text{arange}$, we need to compute an FFT. The FFT is computed on a region having size $|\text{supp } \tilde{g}(\vec{x})|^N$, and the lattice spacing in this region is $2\pi/k_{\max} = O(1/k_{\max})$. Thus, there are $O(|\text{supp } \tilde{g}(\vec{x})|^N k_{\max}^N) = M$ data points in this region. The FFT has computational complexity $M \log(M)$. In addition, we need to compute $|A|$ of these FFT's.

Note that this algorithm can be parallelized very easily, simply by having different processors compute the FFT's for different $\vec{a}x_0$.

Remark 2.2 As an example, consider the case when $A = \text{arange} = \{\vec{a} \in \mathbb{Z}^N : \vec{a}x_0 \in [-(L_{\text{int}} + w), (L_{\text{int}} + w)]^N \setminus [-L_{\text{int}}, L_{\text{int}}]^N\}$. Then the size of A is proportional to $||[-(L_{\text{int}} + w), (L_{\text{int}} + w)]^N \setminus [-L_{\text{int}}, L_{\text{int}}]^N|/x_0^N$. If $L_{\text{int}} \gg w$, then this is of order L_{int}^{N-1} , and the computational complexity is $O(L_{\text{int}}^{N-1} k_{\max}^N \log(L_{\text{int}} k_{\max}))$.

We consider this case since this is what the TDPSF requires.

Phase space projections can also be computed. Let $F \subset \mathbb{Z}^N \times \mathbb{Z}^N$ be finite. Let $A = \{\vec{a} \in \mathbb{Z}^N : \exists \vec{b} \in \mathbb{Z}, (\vec{a}, \vec{b}) \in F\}$. Then we provide the phase space projection algorithm:

Algorithm 2.2 *Phase Space Projection Algorithm*

```
def phase_space_projection(grid, F):
    arange = {a in Z^N : exists b in Z^N, (a,b) in F}
    wft_data = wft_coefficients(grid, arange)
    newgrid    //Has the same size as grid, initialized to 0
    buff       //Has the same size as DualWindow

    for (a,b) in arange X [-kmax,kmax]:
        if (a,b) in F: buff[b] = wft_data[a][b]
        else:          buff[b]=0
        buff = inverseFFT(xbuff) * gaussian(sdev)
        newgrid = newgrid + translate(buff, a*x0)
    return newgrid
```

Clearly, the computational complexity of `phase_space_projection(grid,f)` is of the same order as that of `wft_coefficients(grid, arange)`.

2.2 Propagation with Periodic Boundaries: FFT/Split Step Algorithm

The TDPSF is a filtering algorithm, which is built on top of another propagation method which solves (1.1) on a box with periodic boundaries. The exact manner in which this is done is irrelevant for our purposes, provided it is sufficiently accurate. We let `box_propagator` denote the periodic propagation algorithm, which we will take to be spectral propagation for concreteness.

We fix a grid spacing DX , and timestep DT . The object `grid` is an N dimensional array of size $[2L_{\text{comp}}/DX]^N$. This corresponds to a lattice spacing in momentum of $2\pi/L_{\text{comp}}$, with maximal momentum $2\pi/DX$. A common

rule of thumb is that if the problem has a maximal momentum k_{\max} , then $\Delta x = 4\pi/k_{\max}$.

Let `FFT` be the Fast Fourier Transform algorithm, and `inverseFFT` be the inverse FFT. Let `NLIN(grid,time)` be the numerical implementation of the nonlinearity (which may depend on time).

Finally, `outputstream` is the input to a stream which passes the numerical solution to the appropriate handlers. The handlers are, e.g., programs which graph the data, compute propagation observables, store it to the disk, etc.

Algorithm 2.3 *Split Step Propagation Algorithm*

```
def box_propagator(grid,t_init, t_final,outputstream):
    for j in t_init/DT ... t_final / DT:
        grid = grid * exp(i * NLIN(grid,j*DT) * DT/2)
        grid = FFT(grid)
        grid = grid * exp(i * (1/2)k^2 * DT)
        grid = inverseFFT(grid)
        grid = grid * exp(i * NLIN(grid,j*DT) * DT/2)
        outputstream.append(grid,j*DT)
    return grid
```

The computational complexity of Algorithm 2.3 is

$$O([(t_{\text{final}} - t_{\text{init}})/DT]M^N \ln M)$$

per timestep (with M the number of data points on the grid, per dimension). To resolve spatial scales of order L_{int} and frequencies up to k_{\max} , $M \sim L_{\text{int}}k_{\max}$. Thus, split step propagation has time complexity $O(L_{\text{int}}^N k_{\max}^N \log(L_{\text{int}}k_{\max}))$ per timestep. It is also second order in DT , and third order if (1.1) is linear. Algorithm 2.3 is by now a textbook result [4], so we will not discuss it further.

2.3 The TDPSF Algorithm

The TDPSF algorithm consists of applying the phase space projection operator, implemented using Algorithm 2.2 to solutions of (1.1) periodically in time to filter off outgoing waves. The region of phase space we project onto is waves which are not outgoing.

Outgoing waves are defined to be gaussians $\phi_{(\vec{a},\vec{b})}(\vec{x})$ with $\vec{a}x_0 \in [-(L_{\text{int}} + w), (L_{\text{int}} + w)]^N \setminus [-L_{\text{int}}, L_{\text{int}}]^N$ and which are moving strictly outward under the free flow.

The variable `grid` is some numerical representation of $\psi(\vec{x}, t)$ restricted to the region $[-L_{\text{comp}}, L_{\text{comp}}]^N$ with periodic boundaries. In our case, `grid` consists of equispaced samples of $\psi(x, t)$.

The number `Tstep` is the time between filterings, and should be smaller than $w/3k_{\max}$. The parameters `frm_params` are those parameters which characterize the WFT and the boundary region, namely `(sdev, xs, ks, wb)`.

Algorithm 2.4 *Propagation algorithm*


```

exception CannotFilterException(grid current_grid,
                                number current_time)

Tstep, frm_params, tolerance
strictly_bad_framelets      //a subset of Z^n x Z^n which
                             //consists of framelets which
                             //are all leaving the box.

ambiguous_framelets         //A subset of Z^n x Z^n having
                             //framelets which create errors
                             //but can not be removed.

def propagate_TDPSF(psi0, Tmax, plotter, outputstream):
    grid = psi0
    for j = 0 ... Tmax / Tstep:
        if l2norm(phase_space_projection(grid, ambiguous_framelets))
            > tolerance:
            raise CannotFilterException(grid, j*Tstep)
        grid = grid - phase_space_projection(grid,
                                              strictly_bad_framelets)
        grid = box_propagator(grid, j*Tstep, (j+1)*Tstep, outputstream)
    return grid

```

Thus, all that remains is to determine which framelets are members of `strictly_bad_framelets`, that is to say which framelets are leaving the box.

For a given (\vec{a}, \vec{b}) , this can be determined easily, by a direct calculation based on (1.3). This is done in [26] for $s = 0, 1$, and other cases can be done with the help of Maple/Mathematica.

The end result of the calculation is the following. Define $R_{\vec{b}}(t)$ by

$$R_{\vec{b}}(t) = \sqrt{\sigma^2 + t^2/\sigma^2} (\Gamma^{-1}(N/2, 2\epsilon^2\pi^{N/2}/|S^{N-1}|))^{1/2} \quad (2.7a)$$

if we measure the error in $L^2(\mathbb{R}^N)$ or

$$R_{\vec{b}}(t) = \sqrt{\sigma^2 + t^2/\sigma^2} \max \left\{ \left[\Gamma^{-1} \left(N/2, \frac{\epsilon^2\pi^{N/2}}{2|S^{N-1}|(1+|\vec{b}k_0|_2^2)} \right) \right]^{1/2}, \right. \\ \left. \left[\Gamma^{-1} \left((N+2)/2, \frac{\epsilon^2\sigma^2\pi^{N/2}}{2|S^{N-1}|} \right) \right]^{1/2} \right\} \text{ in } H^1(\mathbb{R}^N) \quad (2.7b)$$

if we measure the error in $H^1(\mathbb{R}^N)$.

The function $\Gamma^{-1}(a, x)$ is the inverse function of $x \mapsto \Gamma(a, x)$, with $\Gamma(a, x)$ the complementary incomplete Gamma function. This definition implies that all the mass (up to a tolerance ϵ) of $e^{i(1/2)\Delta t}\phi_{(\vec{a}, \vec{b})}(\vec{x})$ is, at time t , contained in a ball of radius $R_{\vec{b}}$ about the point $\vec{a}x_0 + \vec{b}k_0t$. That is:

$$\left\| e^{i(1/2)\Delta t}\pi^{-N/4}\sigma^{-N/2}e^{ik_0\vec{b}\cdot\vec{x}}e^{-|\vec{x}-\vec{a}x_0|_2^2/2\sigma^2} \right\|_{H^{0,1}(B(t)^C)} \leq \epsilon \quad (2.8a)$$

$$B(t) = \{x : |\vec{a}x_0 + \vec{b}k_0t - \vec{x}|_2 \leq R_{\vec{b}}(t)\} \quad (2.8b)$$

Thus, if $B(t)$ does not intersect $[-L_{\text{int}}, L_{\text{int}}]^N$, this framelet is strictly bad.

Similar calculations can be done in H^s , although $R_{\vec{b}}$ must be redefined (and now depends on \vec{b}).

Thus, given the result of this calculation, we simply set **strictly_bad_framelets** to be the set of $(\vec{a}, \vec{b}) \in \mathbb{Z}^N \times \mathbb{Z}^N$ such that:

1. $\vec{a}x_0 \in [-(L_{\text{int}} + w), (L_{\text{int}} + w)]^N \setminus [-L_{\text{int}}, L_{\text{int}}]^N$
2. $B(t)$ does not intersect $[-L_{\text{int}}, L_{\text{int}}]^N$

The set **ambiguous_framelets** is the set of framelets for which $B(t)$ intersects $[-L_{\text{int}}, L_{\text{int}}]^N$, but also intersects $\mathbb{R}^N \setminus [-(L_{\text{int}} + w), (L_{\text{int}} + w)]^N$. That is to say, these are framelets with both incoming and outgoing components.

A calculation based on (1.3) shows that these consist of framelets with either low velocities, or framelets which are located on the boundary but are moving tangentially to the boundary.

To assess the time complexity of the TDPSF algorithm, we recall remark 2.2, which says that when $L_{\text{int}} \gg w$, the cost of computing **phase_space_projection(...)** is only $O(L_{\text{int}}^{N-1} k_{\text{max}} \log(L_{\text{int}} k_{\text{max}}))$. Thus, in this case, we find that the added complexity of TDPSF propagation over the Split Step algorithm is of lower order than the Split Step itself. However the constant is significantly larger in our experiments, so on a small grid the TDPSF propagator is slower than FFT/Split Step propagation.

We discuss some possible improvements on this algorithm in section 5.

3 Numerical Examples

In this section we discuss the results of our numerical tests.

The TDPSF algorithm is built in the program Kitty. Kitty is written in Python, with C extensions, calling the external libraries FFTW [14], Numarray and Matplotlib. The external programs gnuplot, ImageMagick and gifsicle were also used for making graphs/movies.

Kitty is licensed under the GPL. It is very much a work in progress, and has little documentation and minimal user interface (an end-user version is currently in progress).

Various test cases, spanning many types of parameters, are also available for download from the author's webpage, <http://math.rutgers.edu/~stucchio>.

3.1 $T + R = E$: Simple Tests

The standard method for testing absorbing boundaries is simply to throw coherent states (which are well localized in frequency) at the boundary and compute transmission (T) and reflection (R) coefficients. The sum $T + R$ is then taken to be the error associated to that particular absorbing boundary condition.

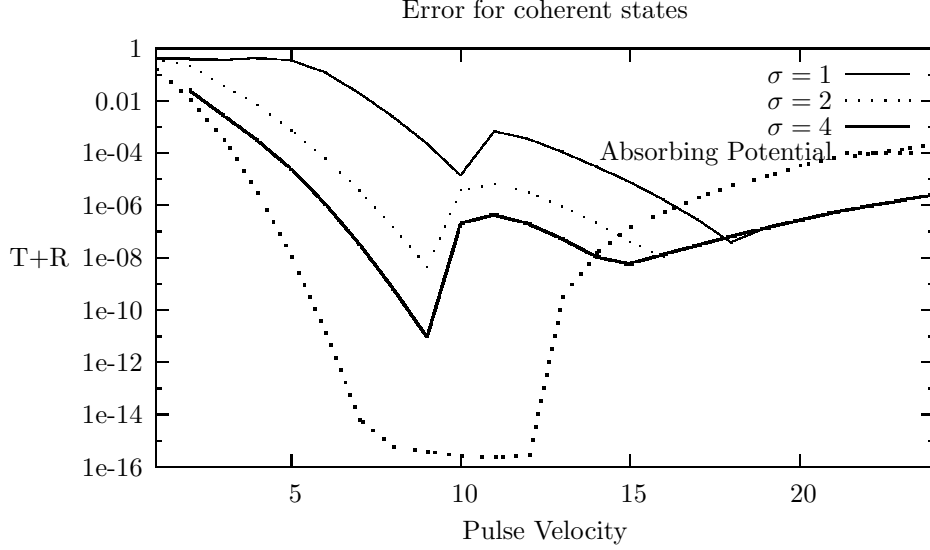


Figure 1: A graph of $T + R$ vs the velocity of an outgoing pulse. Our results appear comparable to an absorbing potential.

This is a useful test, although it is by no means completely characterizes the errors (see section 3.2). We performed the following numerical experiment. The free Schrödinger equation (i.e. $g(t, \vec{x}, \psi(x, t)) = 0$) was solved on the box $[-25.6, 25.6]$ with TDPSF boundaries on the region $[-25.6, -12]$ and $[12, 25.6]$. The initial condition was taken to be $\psi(x, 0) = e^{-x^2/4}e^{ivx}$, with v ranging from 1 to 25. After the initial condition was given sufficient time to wrap around the computational domain, the mass inside the region $[-10, 10]$ was measured, and the result is graphed in Figure 1. This was done with the WFT frame using $\sigma = 1, 2, 4$. The results are comparable to the complex absorbing potential $V(x) = -25ie^{-(x-25.6)^2/16}$, which is also shown in Figure 1. The width of the complex potential was chosen so that its spatial extent is comparable to the width of the TDPSF used.

This particular example demonstrates no major advantage of the TDPSF over the absorbing potential. The TDPSF works better for some velocities, but not all. The advantage of the TDPSF is not that it successfully dissipates outgoing waves. The advantage of the TDPSF is that it does not dissipate incoming waves. An example of this will be demonstrated in the next section.

3.2 $T + R \neq E$: Medium Range Potentials

The main problem associated with an absorbing potential or PML is that not all waves located near the boundary are outgoing. Some waves are incoming,

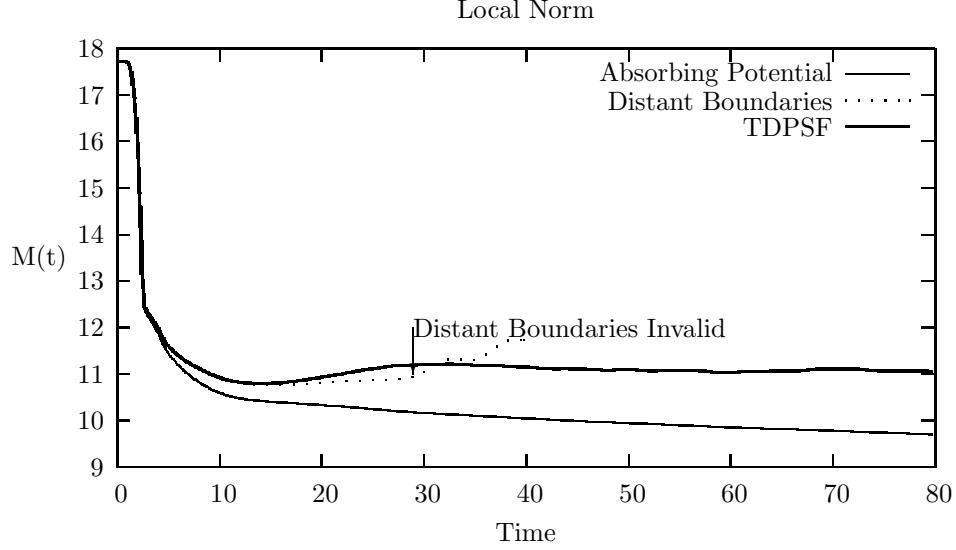


Figure 2: A graph of $M(t) = \|\psi(x, t)\|_{L^2([-10, 10]^2)}$ vs t . The distant boundary simulation is invalid at time $t = 29$, due to the fact that the outgoing pulse returns at this time.

and should not be dissipated.

Consider the following linear Schrödinger equation (with $(\vec{x}, t) \in \mathbb{R}^{2+1}$):

$$\begin{aligned} i\partial_t \psi(x, t) &= \left[-(1/2)\Delta - \frac{15}{0.05|\vec{x}|_2^2 + 1} \right] \psi(x, t) \\ \psi(x, 0) &= e^{i7x_2} e^{-|\vec{x}|_2^2/20} + e^{i4x_1} e^{-|\vec{x}|_2^2/20} \end{aligned} \quad (3.1)$$

The initial condition consists of two coherent states of equal mass, one with velocity 4 and one with velocity 7. The notable fact about this particular potential is that the fast gaussian has enough kinetic energy to (mostly) escape from the binding potential. The slow gaussian does not. The slow gaussian moves toward the boundary, turns around and returns.

The problem with the absorbing potential approach is that the absorbing potential does not distinguish between incoming and outgoing waves. It dissipates everything on the boundary including the waves that should have returned. This will occur even if one can construct a perfectly reflectionless absorbing potential.

We ran three simulations of (3.1). The first was performed using the TDPSF with $\sigma = 2.0$, $x_0 = 0.8$ and $k_0 = 2\pi/12.8 = 0.491$. The region of computation was $[-25.6, 25.6]^2$. The second was performed (on the same region) with an absorbing potential

$$V_1(\vec{x}) = -20ie^{-(\vec{x}_1 \pm 25.6)^2/36} - 20ie^{-(\vec{x}_2 \pm 25.6)^2/36}.$$

The third was solved with periodic boundary conditions on the region $[-102.4, 102.4]^2$. This boundary is sufficiently distant so that the outgoing waves cannot return to the origin for a time $204.8/7.0 \approx 29$. Thus, we will take the distant boundaries simulation as our benchmark, at least for $t \leq 29$.

After $t = 29$, we have some qualitative knowledge of the behavior. We expect that the solution consists of continuum and bound states. Over a short time, the continuum will disperse, leaving only the bound states. The bound states will remain forever.

In all three cases, the quantity $M(t) = \|\psi(x, t)\|_{L^2([-10, 10]^2)}$ was computed. The simulation using the TDPSF agreed with the simulation on the larger region to within 1.25% for $t < 29$. The simulation using complex potentials had an error of 4% for $t < 29$. For $t > 29$, no exact solution is available for comparison.

However, we will compare the two cases as follows. The absorbing potential appears to be dissipating part of the solution, while the TDPSF is not. Figure 2 shows that the TDPSF yields qualitatively correct (bound) behavior, while the absorbing potential displays incorrect (dissipative) behavior. We believe that this dissipation will continue with time, until bound states with energy near $E = 0$ are completely dissipated.

The reason the TDPSF performs better than the complex potential is that it distinguishes outgoing waves from incoming waves. The TDPSF only removes waves which sit on the boundary and are also outgoing with sufficiently high velocity. The trapped waves, although they sit on the boundary, do not have high outgoing velocity, and thus are not removed. The complex potential, in contrast, dissipates waves which should return.

3.2.1 A Subtle Failure

This problem is more subtle than it appears to be. Although in the given example we can determine that the dissipation is artificial, we cannot always do so. Consider a similar problem, but one in which the dynamics support exponentially decaying quasi-bound states (a common occurrence in atomic physics and elsewhere). In this case, the qualitative behavior of the true solution and the absorbing potential are the same; only the rate of decay is wrong. This is a serious worry if calculating the decay rate is the primary goals of the simulation.

In contrast, when the TDPSF fails due to a buildup of slowly moving framelets (the primary mode of failure unique to our method), it fails gracefully. That is, it raises an exception and notifies the user, which is preferable to returning incorrect results.

3.3 Soliton Filtering

Consider the nonlinearity, $g(t, \vec{x}, \psi(\vec{x}, t)) = -|\psi(\vec{x}, t)|^2$. It is desirable to construct a numerical algorithm which filters outgoing solitons as well as free waves. Although filtering solitons is not the goal of the TDPSF, it turns out that that it works as well as most other methods for that purpose.

The reason for this is that an outgoing soliton with sufficiently high velocity is localized in phase space on outgoing waves. Consider a simple soliton, $\phi(x, v, t) = 2^{-1/2} e^{i(vx + (1-v^2)t)} / \cosh((x - vt))$. A simple calculation shows that for $|k - v| \gg 1$, $\hat{\phi}(k, v, t) \sim e^{-|k-v|}$. Thus, for $k \gg k_{\min}$, this shows that the framelet coefficients of $\phi(x, v, t)$ which are moving too slowly to resolve have exponentially small mass. Thus, under the free flow, this soliton is strictly outgoing.

The soliton is also leaving the box under the full flow $\mathcal{U}(t)$. Although $e^{i(1/2)\Delta t}$ and $\mathcal{U}(t)$ move the soliton very differently (one dispersively, one coherently), they both move it out of the box and in nearly the same direction. For this reason, the TDPSF is expected to filter soliton solutions correctly.

We ran numerical tests to demonstrate this as follows. We solved the (1.1) with $g(t, \vec{x}, \psi(\vec{x}, t)) = -|\psi(\vec{x}, t)|^2$ on the region $[-25.6, 25.6]$. In this simulation, $L_{\text{int}} = 12.0$ and $w = 13.6$. The initial condition was taken to be $\psi(x, 0) = 2^{-1/2} e^{ivx} / \cosh(x)$ for $v = 1..15$.

The TDPSF was used with $T_{\text{step}} = 0.08/v$, $x_0 = 0.20$, $k_0 = 2\pi/3.2$, and $\sigma = 1, 2, 3$. We measured the following quantity:

$$E(v) = \sup_{t < 200/v} \frac{\|\psi(x, t) - \psi_{ex}(x, t)\|_{L^2([-10, 10])}}{\|\psi_{ex}(x, 0)\|_{L^2(\mathbb{R})}} \quad (3.2)$$

The function $\psi_{ex}(x, t)$ is the exact solution. The result of this experiment is plotted in figure 3.3. The time $200/v$ was chosen since it is more than enough time for errors to return to the region $[-10, 10]$. We believe the error floor near 10^{-10} visible in Figure 3.3 is due to underlying machine errors, as well as certain approximations we made when computing the WFT.

We discuss a possible better way to filter solitons in Section 5.

Remark 3.1 The paper [27] proposes an alternative method of absorbing boundaries (namely the paradifferential strategy), based on a novel method of approximating the Dirichlet-to-Neumann operator. A similar numerical test was performed for those boundary conditions. For a soliton at velocity 15, Szeftel obtained $E(15) = 0.08$ at best. For comparison, we obtain $E(15) = 1.69 \times 10^{-10}$ for $\sigma = 1$ and $E(v) = 1.40 \times 10^{-10}$ for $\sigma = 3$.

Our tests are not directly comparable. Our region of interest was $[-12, 12]$ with TDPSF region on $[-25.6, -12]$ and $[12, 25.6]$, as opposed to Szeftel who used $[-5, 5]$. We used FFT/Split Step propagation for the interior problem, as opposed to the finite elements of [27].

Nevertheless, it is quite surprising that the TDPSF differs from the Dirichlet-to-Neumann boundary by such a large magnitude, because [27] actually takes the nonlinearity into account while the TDPSF assumes the nonlinearity is zero on the boundary.

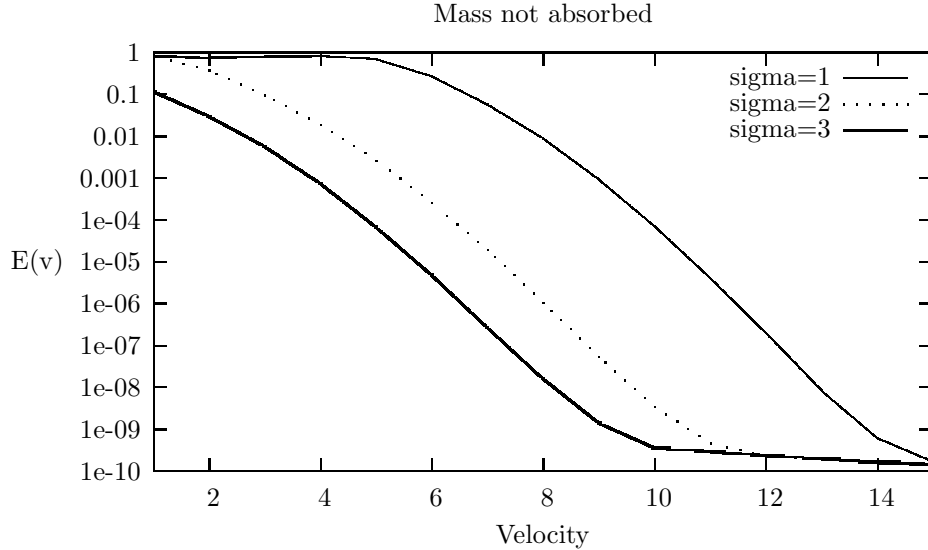


Figure 3: A plot of the error (defined as in (3.2)) as a function of velocity. Note the exponential improvement in accuracy with velocity until the error reaches 10^{-10} .

4 Comparison to Other Methods

4.1 Engquist-Majda type Boundaries, and Dirichlet-to-Neumann Operators

The closest approach to ours is the original Engquist-Majda boundary conditions, found in [13, 11] (see also [1, 2]). The principle that was guiding them was that near the boundary, the geometric optics approximation to wave flow is sufficiently accurate to filter off the outgoing waves.

Our result is a direct analogue of this - the gaussian framelet elements behave (under the free flow) like classically free particles. We use a different method to filter, but the guiding principle is the same.

In comparison, the approach that is farthest from ours are the various modern extensions to [13]. Modern approaches attempt to construct the exact solution on the boundary, and then impose it as a boundary condition. In principle, this is the best possible approach. However, in practice it is difficult to implement for dispersive equations. This approach is sufficiently difficult that we know of very few approaches for the Schrödinger equation. We briefly mention two major approaches that we are aware of, and remark that only one [27] even attempts to deal with nonlinear equations.

An additional problem is that this approach precludes the use of spectral

methods (e.g. Algorithm 2.3) to solve the interior problem. The FFT naturally imposes periodic boundaries rather than Dirichlet-to-Neumann, thus requiring the use of FDTD or other local methods.

4.1.1 Exact Dirichlet-Neumann maps for the Schrödinger Equation

To deal with the free Schrödinger equation (no nonlinearity or potential), Lubich and Schädle [18, 21] constructed an approximation to the exact integral kernel of the Dirichlet-Neumann operator based on a piecewise exponential approximation (in time). This approach appears to work nicely for the free Schrödinger equation, although it is uncertain that it could be applied to the full Dirichlet-to-Neumann operator of a nonlinear equation or medium range problem.

4.1.2 Paradifferential Strategy

The only fully nonlinear Dirichlet-to-Neumann operator that we are aware of was constructed by J. Szeftel in [28]. Szeftel constructs the Dirichlet-to-Neumann operator by a modified version of the paradifferential calculus (see references in [28]). His methodology is demonstrated in 1 space dimension, with a nonlinearity that is C^∞ in x , $\psi(\vec{x}, t)$ and $\partial_x \psi(\vec{x}, t)$. He proves local well posedness of (1.1) with his boundary conditions, assuming H^6 regularity of the initial data.

However, extensions to \mathbb{R}^N appear highly nontrivial. The assumptions are significantly stronger than ours, and there are no error bounds. The numerical experiments look promising and the results appear accurate for radiative problems (see also Remark 3.1).

4.2 Absorbing Potentials/ PML

4.2.1 Absorbing Potentials

Absorbing (complex) potentials, described in [19], are the current “industry standard”. One can add a dissipative term $-ia(x)\psi(\vec{x}, t)$ to the right side of (1.1) and solve it on the region $[-(L_{\text{int}} + w), (L_{\text{int}} + w)]^N$. The function $a(x)$ is a positive function supported in $[-(L_{\text{int}} + w), (L_{\text{int}} + w)]^N \setminus [-L_{\text{int}}, L_{\text{int}}]^N$. This has the effect of (partially) absorbs waves which have left the domain of interest, although it might create spurious reflections. This approach is the mainstay of absorbing boundaries, being simple to understand, simple to program, as well as being compatible with spectral methods.

The potential $a(x)$ must be tuned to the given problem. Given k_{\min}, k_{\max} , one must select the height and width of the absorber so that it kills most of the wave between k_{\min} and k_{\max} . Waves with momentum lower than k_{\min} are mostly reflected, and waves with momentum higher than k_{\max} are mostly transmitted and wrap around the computational domain.

Heuristic calculations and numerical experiments suggest that the absorber must have width proportional to $Ck_{\max} \ln(\epsilon)/k_{\min}$, with C depending on the precise shape of the potential. In contrast, our method works on a boundary layer of width $C \ln(\epsilon)/k_{\min}$, which is smaller by a factor of k_{\max} .

An additional problem with absorbing potentials is that they kill everything on the boundary. This poses a fundamental limitation on their use, especially in problems where the nonlinearity creates long range effects as in Section 3.2.

4.2.2 Perfectly Matched Layers

Perfectly Matched Layers (PML) are a variation on this approach, proposed in [3] for the Schrödinger equation (see also [3], where the PML was introduced). In [17] they are tested for the 1 dimensional free Schrödinger equation, with reasonable results.

The PML consists of adding a term $-ia(x)(1/2)\Delta\psi(\vec{x},t)$ to the right side of (1.1) instead of merely $-ia(\vec{x})\psi(\vec{x},t)$. If $a(\vec{x})$ is chosen carefully, one can completely eliminate reflections at the interface (the boundary of $\text{supp } a(\vec{x})$) for certain frequencies. It also has the property of dissipating high frequency waves more strongly than low frequency ones, thereby eliminating problems due to high frequencies inherent in the absorbing potential approach.

The PML has drawbacks, of course. The PML has the same problem as complex absorbing potentials with regards to dissipating incoming waves on the boundary. Some PML methods are unstable [20]. The PML method for the Schrödinger equation is still very much undeveloped. This makes a more detailed comparison difficult to make.

5 Outlook

Our method is likely to be as versatile and general as the gaussian beam method of harmonic analysis. Extensions and modifications to other sorts of equations are likely to be straightforward, though perhaps using different phase space localization schemes. In particular, we believe the TDPSF can be constructed for the free wave equation in arbitrary dimension, replacing gaussians by curvelets [5, 6]

Another advantage to our method is that when it does fail, it fails gracefully. The main mode of failure is for too many gaussian's to be generated in the region $\vec{b}k_0 \approx 0$. If this occurs, the algorithm is aware of it and raises an exception. We are currently developing a multiscale algorithm to deal with this problem (see below)[25].

Finally, we believe the TDPSF provides a natural means for coupling a classical system governed by a transport equation to a quantum system governed by the Schrödinger equation.

5.1 Classical trajectories

One obvious improvement to our algorithm is useful for dealing with Hamiltonians of the form $H = -(1/2)\Delta + V(x) + f(|\psi(\vec{x},t)|)$ with $V(x)$ a smooth, localized potential. Instead of trying to determine whether the free trajectory of a given framelet, namely $\vec{a}x_0 + \vec{b}k_0t$ is leaving the box sufficiently rapidly, we

try to determine whether the interacting trajectory $\gamma(\vec{a}x_0, \vec{b}k_0, t)$ is leaving the box. The interacting trajectory is the trajectory obeyed by a classical particle with velocity $\vec{b}k_0$, moving in the potential $V(x)$. Intuitively, this is the right thing to do, although we do not have a proof of this.

This is a logical extension of our method that may allow it to deal with equations for which the boundary dynamics are linear but not free. This is particularly important for the study of realistic Coulombic atoms (where $g(t, \vec{x}, \psi) = -z/|x|$). We believe a similar approach could be applied to the wave equation in a slowly varying stratified media.

5.2 Multiscale resolution of slow waves

One potential unknown factor in our algorithm is k_{\min} , the smallest relevant momentum. If the problem we are given has an unknown k_{\min} , all is not lost.

The problem will appear as follows. Suppose that at some time NT_{step} , we find that the mass of the framelets in `ambiguous_framelets` is not small. The only way to reduce k_{\min} is by increasing σ , the standard deviation of the Gaussian, which also increases the width of the buffer w .

We are investigating a multiscale algorithm, utilizing multiple computational grids which accurately deal with the slower frequencies. We use a tower of grids, having width L_{int} , $2L_{\text{int}}$, etc, with each grid having lattice spacing Δx , $2\Delta x$, etc (thus the computational complexity is linear in the number of grids). If slow waves reach the boundary of the first box, they are filtered, and placed on the interior of the 2'nd box. The second box is twice as large, and has a TDPSF filter width σ twice as large as on the first box, thus allowing slower waves to be filtered. This continues until the desired accuracy is reached. Numerical Experiments suggest that this can decrease the error due to slow waves (by a factor of 50 or more), and we plan to investigate this further.

5.3 Soliton Filters

We propose that a practical way to filter outgoing solitons (including those with low velocities) is simply to identify them and remove them. That is, at a time T_{step} , we determine whether $\psi(x, T_{\text{step}})$ might have a soliton located near the boundary. If so, use the decomposition $\psi(x, T_{\text{step}}) = S(x) + R(x)$, where $S(x)$ is the soliton and $R(x)$ is the remainder. We then determine whether $S(x)$ is outgoing. If it is, we then set $\psi(x, T_{\text{step}+}) = R(x)$. Thus, the soliton has been filtered.

This depends on an explicit knowledge of what solitons look like. But that information is available in many cases of practical interest (being the solution of an elliptic problem), so it is not an unreasonable demand.

Acknowledgements: We thank O. Costin and M. Kiessling for useful discussions, and R. Falk for reading the manuscript. This work was supported by NSF grant DMS01-00490. Any opinions, findings, conclusions or recommendations expressed in this material are those of the authors and do not necessarily reflect the views of the National Science Foundation.

References

- [1] Alvin Bayliss and Eli Turkel. Radiation boundary conditions for wave-like equations. *Comm. Pure Appl. Math.*, 33(6):707–725, 1980.
- [2] Alvin Bayliss and Eli Turkel. Outflow boundary conditions for fluid dynamics. *SIAM J. Sci. Statist. Comput.*, 3(2):250–259, 1982.
- [3] Jean-Pierre Berenger. A perfectly matched layer for the absorption of electromagnetic waves. *J. Comput. Phys.*, 114(2):185–200, 1994.
- [4] John P. Boyd. *Chebyshev and Fourier Spectral Methods*. Dover Publications, Mineola, NY, 2001.
- [5] Emmanuel Candès and Laurent Demanet. Curvelets and Fourier integral operators. *C. R. Math. Acad. Sci. Paris*, 336(5):395–398, 2003.
- [6] Emmanuel J. Candès and Laurent Demanet. The curvelet representation of wave propagators is optimally sparse. *Comm. Pure Appl. Math.*, 58(11):1472–1528, 2005.
- [7] Ingrid Daubechies. Time-frequency localization operators: a geometric phase space approach. *IEEE Trans. Inform. Theory*, 34(4):605–612, 1988.
- [8] Ingrid Daubechies. *Ten lectures on wavelets*, volume 61 of *CBMS-NSF Regional Conference Series in Applied Mathematics*. Society for Industrial and Applied Mathematics (SIAM), Philadelphia, PA, 1992.
- [9] Ingrid Daubechies and A. Grossmann. Frames in the Bargmann space of entire functions. *Comm. Pure Appl. Math.*, 41(2):151–164, 1988.
- [10] Ingrid Daubechies, A. Grossmann, and Y. Meyer. Painless nonorthogonal expansions. *J. Math. Phys.*, 27(5):1271–1283, 1986.
- [11] Björn Engquist and Andrew Majda. Absorbing boundary conditions for numerical simulation of waves. *Proc. Nat. Acad. Sci. U.S.A.*, 74(5):1765–1766, 1977.
- [12] Björn Engquist and Andrew Majda. Absorbing boundary conditions for the numerical simulation of waves. *Math. Comp.*, 31(139):629–651, 1977.
- [13] Björn Engquist and Andrew Majda. Radiation boundary conditions for acoustic and elastic wave calculations. *Comm. Pure Appl. Math.*, 32(3):314–358, 1979.
- [14] Matteo Frigo and Steven G. Johnson. The design and implementation of FFTW3. *Proceedings of the IEEE*, 93(2):216–231, 2005. special issue on “Program Generation, Optimization, and Platform Adaptation”.
- [15] Dan Givoli and Beny Neta. High-order non-reflecting boundary scheme for time-dependent waves. *J. Comput. Phys.*, 186(1):24–46, 2003.

- [16] Thomas Hagstrom. Radiation boundary conditions for the numerical simulation of waves. In *Acta numerica, 1999*, volume 8 of *Acta Numer.*, pages 47–106. Cambridge Univ. Press, Cambridge, 1999.
- [17] Thomas Hagstrom. New results on absorbing layers and radiation boundary conditions. In *Topics in computational wave propagation*, volume 31 of *Lect. Notes Comput. Sci. Eng.*, pages 1–42. Springer, Berlin, 2003.
- [18] Christian Lubich and Achim Schädle. Fast convolution for nonreflecting boundary conditions. *SIAM J. Sci. Comput.*, 24(1):161–182 (electronic), 2002.
- [19] Daniel Neuhauser and Micheal Baer. The time-dependent schrodinger equation: Application of absorbing boundary conditions. *J. Chem. Phys.*, 90(8), 1989.
- [20] D. Gottlieb S. Abarbanel and J.S. Hesthaven. Long time behavior of the perfectly matched layer equations in computational electromagnetics. *Journal of Scientific Computing*, 17(1), 2002.
- [21] Achim Schädle. Non-reflecting boundary condition for a Schrödinger-type equation. In *Mathematical and numerical aspects of wave propagation (Santiago de Compostela, 2000)*, pages 621–625. SIAM, Philadelphia, PA, 2000.
- [22] Achim Schädle. Non-reflecting boundary conditions for the two-dimensional Schrödinger equation. *Wave Motion*, 35(2):181–188, 2002.
- [23] I. M. Sigal and A. Soffer. Asymptotic completeness of short-range many-body systems. *Bull. Amer. Math. Soc. (N.S.)*, 14(1):107–110, 1986.
- [24] I. M. Sigal and A. Soffer. The N -particle scattering problem: asymptotic completeness for short-range systems. *Ann. of Math. (2)*, 126(1):35–108, 1987.
- [25] A. Soffer and C. Stucchio. Multiscale resolution of low frequencies for time dependent dispersive waves. *in preparation*.
- [26] A. Soffer and C. Stucchio. Time dependent phase space filters: Nonreflecting boundaries for semilinear schrodinger equations. *preliminary version*.
- [27] Jeremie Szeftel. Absorbing boundary conditions for nonlinear schrodinger equations. *preliminary version*.
- [28] Jérémie Szeftel. Design of absorbing boundary conditions for Schrödinger equations in \mathbb{R}^d . *SIAM J. Numer. Anal.*, 42(4):1527–1551 (electronic), 2004.